PROCEEDINGS, 51st Workshop on Geothermal Reservoir Engineering
Stanford University, Stanford, California, February 9-11, 2026
SGP-TR-230

Decimeter-scale Laboratory Investigation of Fracture Thermal Energy Storage

Ambroise Mathey, Salomé Pierre, Andreas Möri and Brice Lecampion

Geo-Energy Lab, Ecole Polytechnique de Lausanne, Station 18, CH-1015 Lausanne, Switzerland

ambroise.mathey@epfl.ch, brice.lecampion@epfl.ch

Keywords: Fracture thermal energy storage (FTES), Hydraulic fracture, Fracture transmissibility, Model calibration, Heat transfer.

ABSTRACT

Fracture Thermal Energy Storage (FTES) stores and recovers heat in low-permeability rock by circulating fluid through hydraulically created fractures that act as transient heat exchangers. We report decimeter-scale laboratory FTES experiments on 25-cm cubic granite and gabbro blocks containing one or three fractures created by hydraulic fracturing. Thermal charge–discharge cycles are performed by circulating hot and cold water between a central injection well and production wells while varying inlet temperature and flow rate, and monitoring inlet/outlet temperatures and the block surface temperature fields. The early-time mean surface warming is approximately linear and scales with injected thermal power (constant flow rate at fixed inlet temperature). The hydraulic response evolves during heating: at constant flow rate, injection pressure increases as the block warms and is higher for higher inlet temperatures, consistent with a temperature-dependent reduction of effective fracture transmissivity. Long injections reach a quasi-steady regime where input thermal power is balanced by boundary heat losses to the laboratory environment; this regime enables estimation of loss power and cumulative lost energy. These measurements constrain key parameters and would enable calibration and validation of a hydrothermal model accounting for the conductive host-rock boundary conditions expected in a field-scale FTES system. It provides quantitative insight into how fracture transmissibility and connectivity affect FTES efficiency.

1. INTRODUCTION

Underground thermal energy storage (UTES) is increasingly relevant for balancing mismatches between energy supply and demand over seasonal timescales. The most common UTES approaches are Aquifer Thermal Energy Storage (ATES) and Borehole Thermal Energy Storage (BTES). ATES is widely deployed and has been reviewed extensively (Fleuchaus *et al.* 2018), while optimal and sustainable use of the subsurface for ATES depends strongly on local hydrogeological and operational constraints (Bloemendal *et al.* 2014). In many settings, particularly in shallow crystalline rocks where intrinsic permeability is low and suitable aquifers are absent, the range of UTES options becomes limited, motivating concepts that rely on engineered permeability rather than native groundwater flow.

Fracture Thermal Energy Storage (FTES) is an alternativeoption which consists in creating or stimulating fractures to form high-surface-area flow paths in otherwise tight rock, enabling high heat-transfer rates despite low rock thermal conductivity and limiting convective heat losses to the surrounding formation (Hellström *et al.* 2001), The concept originates from early work on hydraulic fracturing for heat storage and extraction in crystalline rocks (Larson *et al.* 1984) and was formalized as the HYDROCK concept for seasonal thermal energy storage (Hellström *et al.* 2001). Subsequent modelling studies comparing HYDROCK-type systems to large BTES configurations suggested potential efficiency gains of FTES (on the order of 10–20% in the reported comparison), while also highlighting that produced temperatures can decline over weeks and that further design optimisation is needed (Hellström *et al.* 2001). Field tests in Norway demonstrated that multiple parallel fractures can be created and circulated but also showed that achieving adequate production rates can be a key challenge (Ramstad *et al.* 2007). More recent work has explored feasibility in other high-latitude crystalline settings, but laboratory experimental investigations of the coupled thermal response and long-term flow performance remain limited (Janiszewski *et al.* 2018).

We report laboratory FTES experiments on 25 cm fractured rock blocks (granite and gabbro) designed to quantify thermal and hydraulic responses. Fractures are created under controlled fluid injection, outlet wells are drilled and completed, and thermal charge–discharge cycles are performed by circulating hot and cold water between injection and production wells under various flowrate and inlet-temperature conditions. Inlet/outlet temperatures and dense surface temperature measurements are used to quantify heating rates, thermo-hydraulic responses, spatial heterogeneity of heat exchange, and long-time plateau behavior. Because finite laboratory specimens exchange heat with the lab surrounding, energy recovery metrics are strongly influenced by boundary heat losses; we therefore quantify these losses explicitly and use them to motivate field-relevant modelling with conductive (buried) boundary conditions.

2. MATERIALS AND METHODS

2.1 Specimen preparation and fracture creation

2.1.1 Mechanical setup

The creation of hydraulic fractures was performed in a true triaxial press developed at EPFL Geo-Energy lab. The apparatus enables us to set the two horizontal stresses are equal ($\sigma_1 = \sigma_2$) and greater than the vertical one (σ_3), so that the fracture propagates preferentially in a horizontal plane. The samples used are cubes of 25 cm edge length. Between the pistons and the sample are placed 2 cm thick platens,

which contain electrical feedthroughs that allow the cables from acoustic sensors to exit the frame safely. The injection line enters through the top face of our samples and connects to the injection tool inside the well cored vertically in our sample (see Fig 1 right).

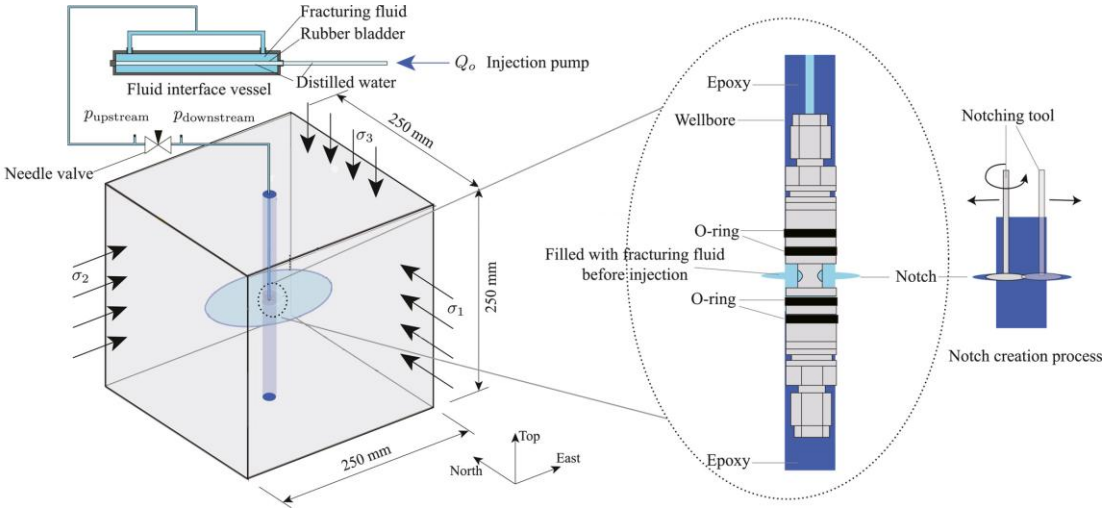

Figure 1 - Left: Schematic of the 25-cm cubic rock specimen in the triaxial. Nine pistons arranged in a 3×3 array apply normal stresses on each face, ensuring uniform confinement. Right: Zoom on the injection tool used for single-fracture experiments. Once positioned at the notch depth, the surrounding well is filled with epoxy to isolate the injection volume and withstand high pressure. (adapted from Liu *et al.* 2022)

2.1.2 Well Coring and completion

The injection wells were cored vertically through the entire height of the samples, with diameters ranging from 1.6 to 2 cm, depending on the specimen. A notch was created on the surface of the well at the fracture's desired heights. Each well was later completed using epoxy resin to seal the completion tool(s) inserted at the level of each notch (see Fig 1). The injection fluid was delivered through a stainless-steel tube (1.6 mm in internal diameter) inserted into the completion and connected to the external circuit via the top platen. In the case of three-fracture configuration, 3 injection lines were stacked inside the well (each in front of their own notch). Such a completion design has the added advantage of allowing to perform FTES circulation experiments in one, two or three fractures at a time.

2.1.3 Hydraulic fracturing protocol

Fracture creation for one or three fractures sample follow the same protocol where once the sample is placed in the frame with its sensor, the pistons are activated and the stress applied to each face of the sample are set within a range of 5 to 17.5 MPa depending on experiments. As said before we imposed the vertical stress to be smaller than the 2 horizontal stresses to help propagate horizontal fractures. Once the sample is confined, the injection was made at low flowrates ranging from 0.1 to 0.05 mL/min. The injected fluid, chosen for their high viscosity (glucose: 65 mPa.s and silicone oil: 100 mPa.s), were injected through an interface vessel which allowed for good control of the injected flowrate. Fig 2 presents the pressure curve for an injection of glucose into the 3-fracture sample (corresponding to the top fracture). Following a pressurization phase, the breakdown corresponding to the fracture propagation can be clearly seen.

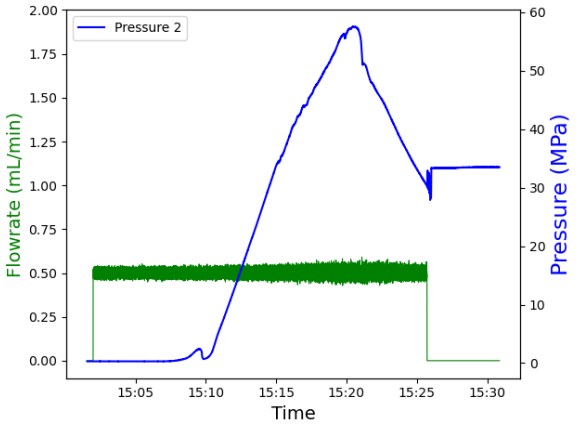

Figure 2 - Injection pressure for the top fracture creation. A clear breakdown pressure corresponding to the fracture propagation is visible.

Although our fracture characterization is limited, based on visual observations of the surface traces on the sample's faces, each fracture can be reasonably approximated as a horizontal planar surface cutting across our 25 cm × 25 cm block. Under this assumption, a conservative lower-bound estimate of the fracture area is simply ATot ≈ 2 × 625 cm² = 1250 cm² per fracture. This estimate does not include any correction for roughness, aperture variations or irregular geometry, because these quantities cannot be directly measured with the available experimental tools. In reality, the effective area in contact with circulating fluid will be larger due to surface asperities, but this cannot be precisely quantified. This provides a geometric constraint for interpreting the thermal response and for the conductive-boundary modelling discussed in Section 5.

2.2 Flow loop, wells and boundary sealing

Once the fractures were created, we cored outlet wellbore(s) that intersected with the fracture(s). In the single fracture samples, a single outlet well was made for each. They were cored vertically in one of the corners of the top face of each block and stopped when it reached the fracture, giving us valuable information about the exact position of the fracture in that area. Those wells were completed just above the fracture with a steel completion tool and epoxy. Fig 4 displays a schematic of the completion for single fracture samples.

For the three-fracture block, we wanted to have more outlet wells, and to be able to control the flow from each fracture independently. To do this, we used the same completion design for the outlet wells as for the injection completion tool and attached temperature sensors that measure the water temperature coming out of the fractures. Three outlet wells were cored vertically from the top face of the sample. Fig 4 (right) displays a schematic of the completion for the three-fracture sample.

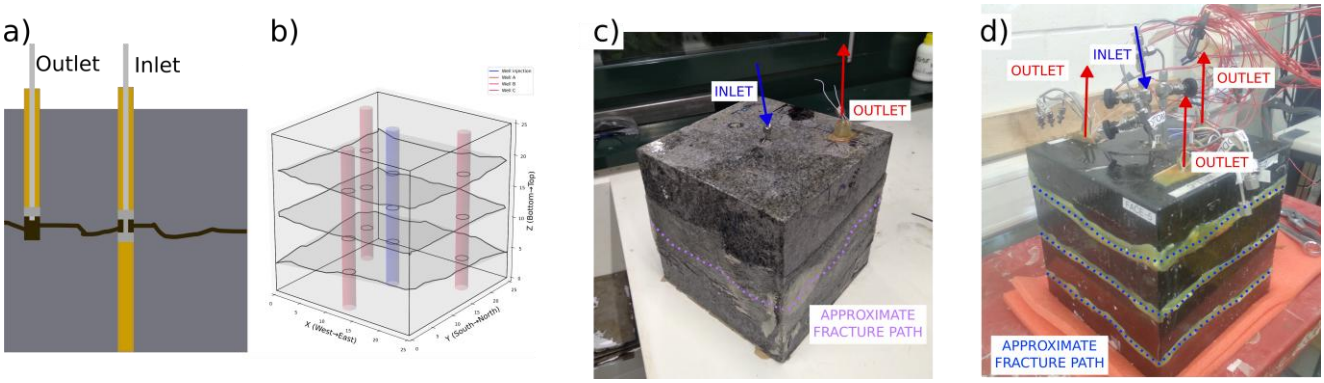

Figure 3 - a) Schematics of the completion of the inlet and outlet wells in a single fracture sample. The yellow filling in each well is epoxy resin, while the dark grey items are the completion tool placed at the bottom of the outlet well and in the middle of the injection well. b) 3D view of the distribution of the outlet wells (in red) in the three-fracture sample. c) LANH-02 samples with inlet and outlet well and sealing of the fracture with epoxy and glass fibre. d) GABB-11 sample with the 3 visible fractures (sealed with epoxy on the sample outer surfaces), 3 inlet and 9 outlet lines (3 per outlet wells).

The fracture(s) intersection with the external faces of the samples were sealed up by using a mix of epoxy and glass fibre to create a closed system where water would only flow out through the designated outlets. In all cases, the sealing eventually leaked, especially when subjected to high pressure over extended periods of time. We therefore removed and reapplied the mix of epoxy and glass fibre when required. The work presented in this paper are based on experiments where no visible external leakage was observed (or where leakage was immediately repaired), so that flow was primarily recovered through the instrumented outlet wells.

2.3 Thermal cycling and temperature monitoring

We monitored temperatures at three locations to characterise thermal loading and recovery. Fluid inlet temperature was recorded just before the tubing entered the sample with a type-J thermocouple (M12JSS-M6-U-200-A from RoHS). Fluid outlet temperature was measured at the bottom of each production well (SMT Ring Terminal Probe ETP-RT-4-20- 10K3A1B from VARIOHM) for the three-fracture setup and type-J thermocouple for the one fracture samples. Finally, rock surface temperature was recorded with an array of thermistor sensors distributed on the faces. The position of these sensors is displayed in Fig 5. Pumps and heaters were automated in LabVIEW, while temperature logging was handled by Arduino MEGA boards.

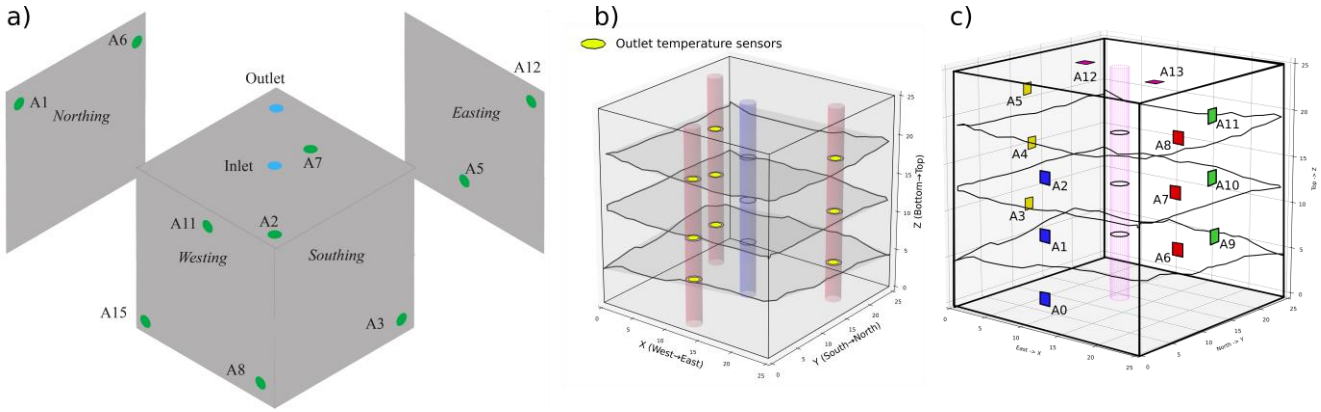

Figure 5 – Location of the surface, inlet and outlet temperature measurements for LANH-02 (a) and GABB-11 (b)(c) samples

The system used resistive heating tapes wrapped around a long section of stainless-steel tubing and regulated by a PID controller (Fig 6). The PID feedback relies on a thermocouple sensor (M12JSS-(M6)-U-200-A from RoHS) installed in the circuit.

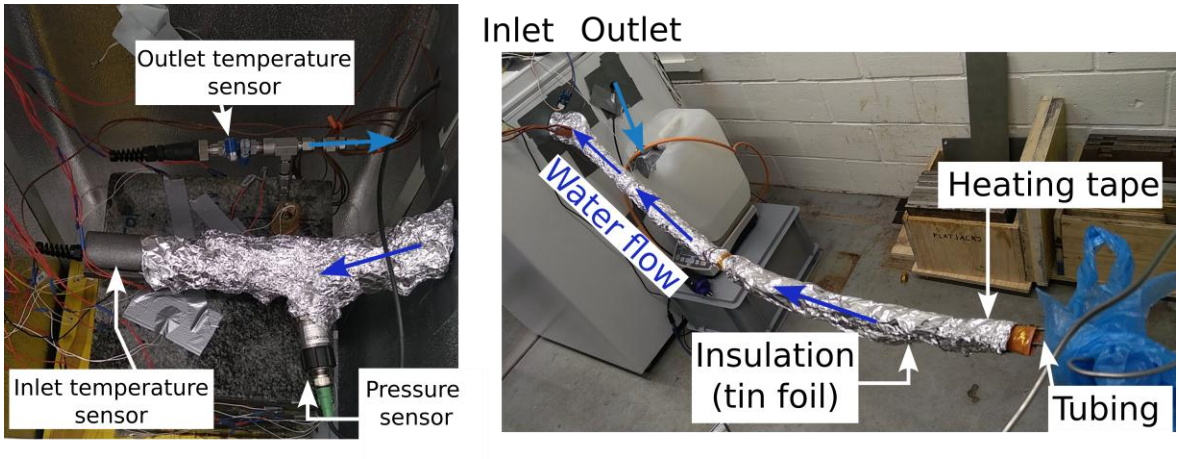

Figure 6– Heating tape system to heat the injection water at a constant temperature. In this system the water flows through a metal tube with heating tape wrapped around it. The heating tape power supply is controlled by a PID controller (feedback controller, not visible in the photos) that monitor the water temperature at the inlet of the sample. It adjusts the heating to automatically maintain the injected fluid temperature constant.

3. TYPICAL EXPERIMENT AND GENERAL BEHAVIOUR

3.1 Typical experiment

A typical FTES experimental sequence consisted of a heating phase, where hot water is injected through the central well and cooled water is collected from the peripheral wells, followed by a pause without flow. The following cooling phase involved injecting room temperature water through the same central well while recovering the heated water at the periphery. The behaviour of the block during a typical experiment can be seen in Fig 7 where the temperature recorded at the surface of the block is plotted as a function of time along with the outlet temperature of the water. This is for an experiment where 80 °C water was injected in the LANH-02 sample at 5 mL/min for 3 hours, paused for 1h30 and room temperature water was injected for another 3 hours.

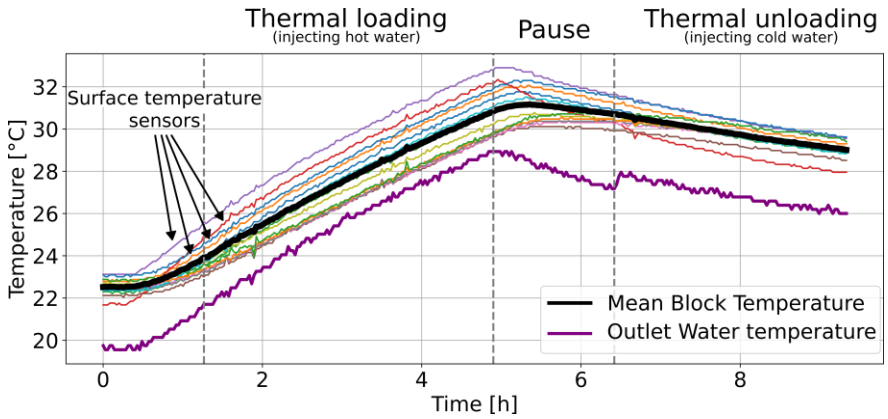

Figure 7- Thermal loading schedule and temperature recording for LANH-02.

3.2 Experiments summary

The experiments reported in this paper are summarized in Table 1. We vary the injection rate, injection temperature, and fracture configuration (single vs. three fractures) while keeping the loading schedule comparable (heating–pause–cooling cycles). This set of tests is used to isolate (i) the effect of injected thermal power on heating rate, (ii) thermo-hydraulic coupling on injection pressure, and (iii) the spatial distribution of heat in the block.

Table 1. Parameters of the experiments presented in this paper

Experiment label	Sample	Fracture	Injection rate	Injection temperature	Cycle duration (heating/pause/cooling/ pause)
lanh-5-150	LANH-02	/	5 mL/min	150 °C	3h/1h30/3h/1h30
lanh-2.5-150	LANH-02	/	2.5 mL/min	150 °C	3h/1h30/3h/1h30
lanh-cycle_9	LANH-02	/	5 mL/min	80 °C	[3h/1h30/3h/1h30] x 9
gabb11-25-3f	GABB-11	All 3	25 mL/min	78 °C	12h/1h/12h/1h
gabb11-25-M	GABB-11	Middle	25 mL/min	78 °C	12h/1h/12h/1h
gabb11-25-B	GABB-11	Bottom	25 mL/min	78 °C	12h/1h/12h/1h

4. RESULTS AND DISCUSSION

We first quantify how injected thermal power controls the early-time heating rate of the block (Section 4.1). We then show that temperature also affects the hydraulic response, with injection pressure evolving during heating at fixed flow rate (Section 4.2). Next, we use the surface thermistor array to discuss where heat is exchanged and why wells and fracture location matter for spatial heterogeneity (Section 4.3). Finally, we focus on the long-time plateau regime, which is governed by boundary losses and provides a way to quantify heat loss to the laboratory (Section 4.4).

4.1 Heating rate scaling

The injection rate controls the rate at which thermal energy is supplied to the fracture network. For a given injection temperature, a higher flow rate corresponds to a larger injected thermal power and therefore a faster heating of the rock volume. Fig 8 illustrates this effect for LANH-02, where 2 experiments were performed at 2 different injection rates with the same inlet temperature (150C).

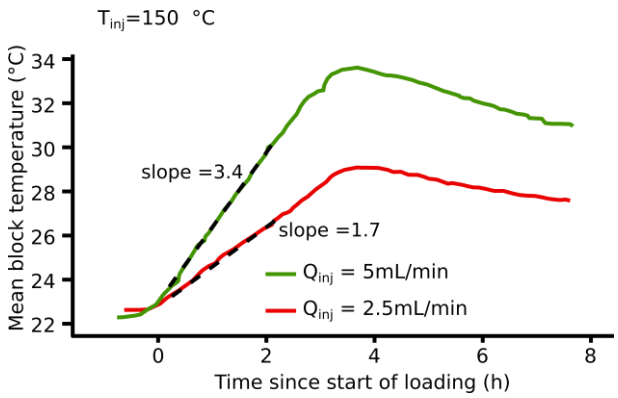

Figure 8 - Average surface temperature of LANH-02 during thermal injections at two flow rates (5 and 2.5 mL/min). The early-time heating is approximately linear, and the heating rate increases with flow rate, consistent with a scaling proportional to the injected thermal power.

During the early phase of heating, the average surface temperature increases approximately linearly with time. The slope of this increase scales with injection rate, confirming that the heating rate is controlled by the injected thermal power. At later times, the curves progressively approach a plateau that reflects a balance between injected power and heat losses (mainly radiation and external convection) together with conductive heat spreading within the block.

4.2 Injection pressure evolution

Thermal effects also influence the hydraulic behaviour of the system. Figure 9 shows three thermal injection experiments performed on the LANH-02 sample at the same flow rate of 5 mL/min but at three different injection temperatures of 75, 80 and 150 °C. The data show two clear features.

First, the experiment with the highest injection temperature systematically exhibits the highest injection pressure. Second, within each individual experiment, the injection pressure increases progressively during heating as the block warms up. Since the flow rate is constant, this increase in pressure reflects a reduction of the effective hydraulic transmissivity of the fracture during heating.

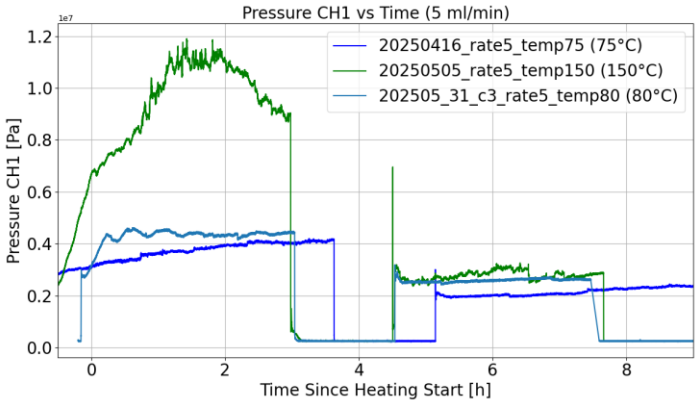

Figure 9 - Injection pressure and block temperature for LANH-02 at a fixed flow rate (5 mL/min) and three inlet temperatures. Higher inlet temperatures yield higher injection pressures, and pressure increases during heating within each experiment, consistent with a reduction in transmissivity as the block warms.

The simplest explanation is thermo-elastic closure: as the block warms, fracture aperture decreases and a higher pressure is needed to maintain the same flow rate. This effect is clearest in low-transmissibility samples such as LANH-02, where small changes in aperture translate into measurable differences in hydraulic resistance. In the present study, the behaviour was not always reproducible across samples, but it is consistent with similar observations made during decameter-scale thermal injection tests recently conducted by PNNL at SURF (Hibbard et al. 2024). The coupling between thermal loading and the evolution of fracture transmissivity is a possibly important effect to account for.

These results illustrate that the hydraulic behaviour of a fracture during thermal injection is sensitive to temperature. Understanding this thermo-hydraulic coupling will be important for evaluating long-term FTES behaviour under repeated charge–discharge cycles. While pressure captures how the fracture transmits flow, it does not tell us where the injected heat is exchanged within the specimen. To interpret heating efficiency and the onset of plateau behaviour, we therefore examine the spatial distribution of surface temperatures.

4.3 Spatial temperature distribution

4.3.1 Inlet and outlet wells contribution to heat exchange

Despite being insulated by epoxy, the injection and production wells play a significant role in the thermal evolution of the block. Their surface area is small compared with that of the fractures (2%), yet they present the largest temperature contrast with the surrounding rock. As a result, they exchange heat with the block, especially the injection well.

In all experiments, the surface temperature measurements showed a clear asymmetry between the upper and lower halves of the block, with higher temperatures observed above the fracture during heating. This anisotropy persisted throughout the hot injection phases and even during the temperature plateau (observed for long experiments), indicating that the wells contribute continuously to the redistribution of heat within the sample. During cooling, the situation was reversed: the top part of the block cooled more rapidly than the lower half, consistent with the wells having strong capacity to exchange heat because of the higher temperature difference.

This effect is illustrated in Fig 10, which displays the evolution of the average block surface temperature and the evolution of the temperature of the upper and lower regions for two representative experiments (performed on LANH-02 and GABB-11). The temperature difference between the two sub-sections of the block does not vanish during steady-state operation, confirming that the wells influence the spatial distribution of heat in our samples. These local exchanges should be much smaller in large-scale field systems, where the ratio between the wells and fractures areas is much smaller. However, it must be taken into account when interpreting our laboratory results and should be included in any numerical modelling of these experiments.

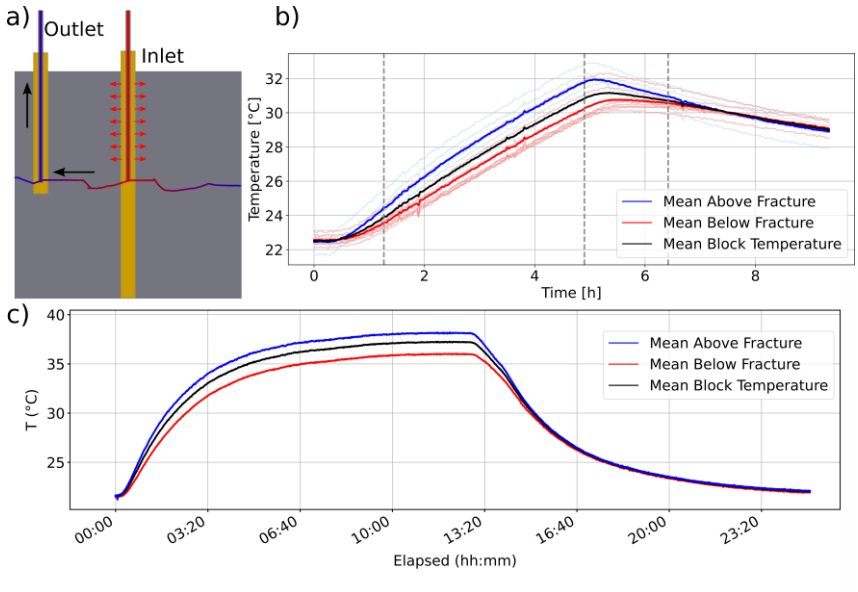

Figure 10 – Evolution of the average block surface temperature and of the temperatures measured on the upper and lower halves of the block for two representative experiments (LANH-02 and GABB-11). The persistent temperature difference between the two regions during heating, plateau, and cooling phases illustrates the significant contribution of the injection and production wells to internal heat exchange.

4.3.2 Roles of fractures

In the case of 3-fracture injection, the spatial distribution of temperature shows that the heat originates from the fracture where the injection takes place. This is displayed in Fig 11 where we plot the temperature of the block for different "slice" of block (section of the block separated by fractures). We define 4 slices A, B, C and D going from bottom to top. The heat propagated from this fracture into the block, confirming that each fracture acts as an independent exchange surface. Even if the overall response of the block appears similar for one or three active fractures, the distribution of temperature within the rock clearly reflects which fracture was used for injection.

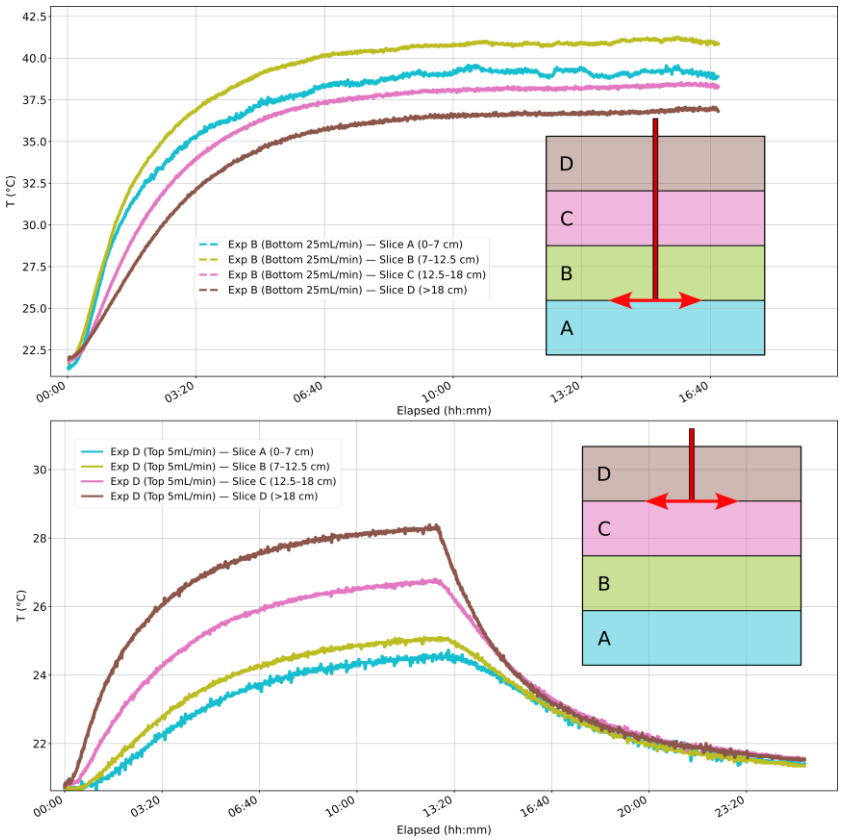

Figure 11 - Spatial distribution of temperature within the GABB-11 block during heating, shown for four slices (A to D, from bottom to top) separated by the fracture planes. The temperature evolution clearly shows that heat originates from the fracture where injection occurs and propagates through the block, confirming that each fracture acts as an independent heat-exchange surface. Although the wells influence the overall temperature field, their effect does not mask the dominant thermal signature of the active fracture.

In this parameter range, the system-level response is dominated by boundary losses and finite block size rather than by the number of active fractures. We are investigating whether in a lower-power regime, the role of individual fractures will become more visible. Another ongoing investigation is the equal split of the flow rate in-between the three fracture. Indeed, in the current setup, when we inject in the three fractures, most of the flow is concentrated in the fracture with the highest permeability (the middle one). We believe that by adjusting the flow rate in each fracture, we could improve the global efficiency of the system. Additional experiments are needed to explore this regime and quantify the specific role of fracture connectivity and transmissibility in the overall heat exchange.

In all cases, the finite size of the laboratory block and its exposed boundaries strongly influence the long-time behaviour: after several hours the surface and outlet temperatures approach a quasi-steady plateau. In the next section, we exploit this plateau regime to quantify boundary heat losses to the laboratory.

4.4 Experimental Plateau Behaviour of the Surface Temperatures

During long heating phases, the surface temperatures systematically follow three successive stages. We use the long-duration GABB-11 experiments to illustrate this three-stage response (Fig. 12).

Immediately after the start of hot-water injection (Fig. 12b), the measured surface temperatures remain essentially unchanged. The thermal perturbation is initially confined to the injection well and the connected fracture, and the thermal front has not yet reached the external faces. Heat is transported advectively along the fracture plane and diffuses conductively into the surrounding rock, but remains local and is not resolved by the surface thermistor array. The duration of this stage depends primarily on fracture transmissivity, injection rate and block size, which together control the propagation speed of the thermal front.

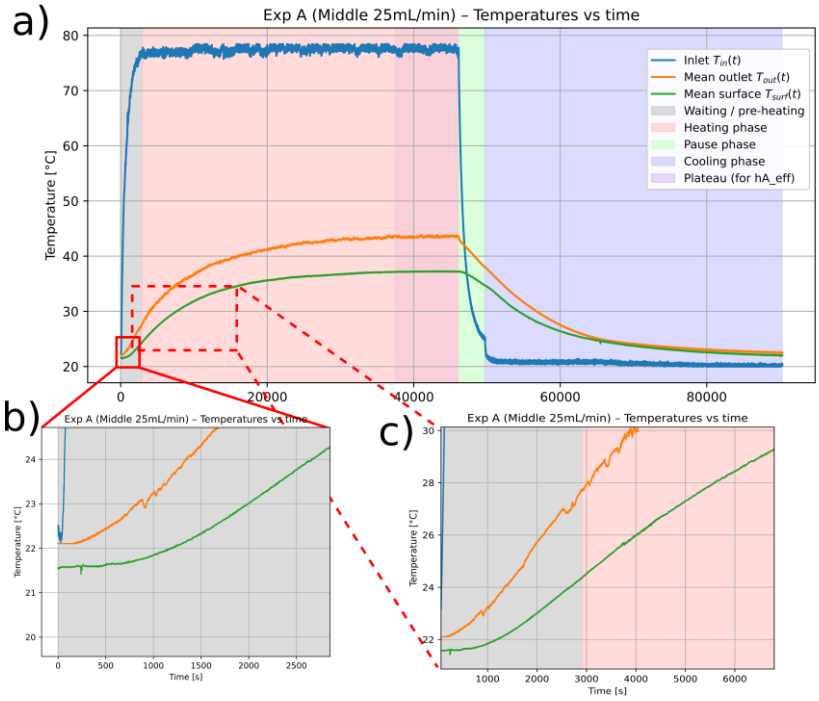

Figure 12 - (a) outlet and mean surface temperature showing plateau for gabb11-25-M; (b) early-time response (stage 1); (c) intermediate quasi-linear warming (stage 2)

Once the thermal front reaches the external surfaces (Fig. 12c), the mean surface temperature increases approximately linearly with time. This regime corresponds to conduction-dominated heat transfer from the heated fracture plane toward the outer faces of the specimen. The slope of this increase defines an effective heating rate of the block and is used in Section 4.1 to compare injection conditions. The duration of this stage and the heating slope depend on the rock thermal diffusivity and on the imposed temperature difference between the injected fluid and the initial block temperature.

At later times, both the outlet temperature and the average surface temperature tend toward a quasi-steady value and evolve only slowly over several hours (Fig. 12a). This plateau results from the competition between heat input from the injected hot water and heat losses from the external surfaces of the block to the laboratory environment. Once these two effects approximately balance, the outlet temperature becomes nearly constant, the mean surface temperature on each face evolves very slowly, and the overall retained energy increases only marginally.

The plateau regime provides a practical way to quantify heat losses to the laboratory. In this quasi-steady state, the rate of change of stored energy in both the fluid and the rock is small, so that the thermal power retained by the system is approximately balanced by the thermal losses at the external boundary: $P_{ret} = P_{loss}$.

Here P_{ret} is the net thermal power transferred from the circulating fluid to the block (i.e., injected power minus produced power), evaluated during the plateau.

We model the losses using a linear heat-transfer law based on the measured average surface temperature:

$$P_{loss} = h_r A_{ext}\left(T_{surf} - T_{lab}\right)$$

where A_{ext} is the external surface area of the block, T_{surf} is the measured average surface temperature, T_{lab} is the laboratory ambient temperature, and h_r is an effective heat-transfer coefficient that aggregates radiative and convective exchanges at the block boundary.

Using the plateau of experiment gabb11-25-M (Fig. 12a), we identify h_r by equating P_{loss} to the plateau value of P_{ret}:

$$h_r = \frac{\langle P_{ret}\rangle_{plateau}}{A_{ext}\left(T_{surf,plateau} - T_{lab}\right)}$$

This yields an effective heat-transfer coefficient $h_r \simeq 9.2$ W.m^{-2}.K^{-1}. We then use this value, together with the measured surface temperature time series, to compute the instantaneous loss power Ploss (t) and the cumulative lost energy

$$E_{loss}(t) = \int_0^t P_{loss}(\tau)d\tau$$

for all experiments.

We are currently using this loss estimate to separate “true storage” from laboratory boundary artefacts and to guide field-relevant numerical modelling in which radiative losses are replaced by conductive heat transfer into a surrounding rock volume.

5. CONCLUSION AND OUTLOOK

Laboratory FTES circulation experiments in fractured 25-cm rock blocks show that the early-time heating rate scales with injected thermal power (controlled by flow rate at fixed inlet temperature). The hydraulic response can also evolve during heating: at constant flow rate, injection pressure tends to increase as the block warms, consistent with a reduction of effective fracture transmissivity. Surface temperature measurements reveal persistent spatial heterogeneity, highlighting the role of wells in redistributing heat at laboratory scale while the dominant thermal signature still originates from the actively injected fracture.

Long-duration experiments reach a quasi-steady plateau in which the retained thermal power is approximately balanced by radiation boundary losses to the laboratory. Using this regime, we quantify the external losses by identifying an effective heat-transfer coefficient ($h_r \approx 9.2$ W.m^{-2}. K^{-1}) and computing instantaneous loss power and cumulative lost energy from the measured surface temperatures.

With losses quantified, we can now move from a laboratory energy budget to one that can be applied to a real FTES configuration, where radiation is negligible, and heat is transferred conductively into the formation. We will therefore use the present dataset to build and calibrate a hydro-thermal model in which the laboratory radiative boundary is replaced by a conductive host-rock boundary. In such a configuration, the surrounding rock progressively warms over repeated cycles, reducing boundary temperature gradients and therefore decreasing losses per cycle; this implies that storage efficiency should increase with time as the system approaches a thermally conditioned state.

Acknowledgements

This work was performed within the Geothermica project DEMO-FTES. Funding from the Geothermica Initiative and the Swiss Federal Office of Energy under grant SI/502470-01 is greatly acknowledged. Extensive discussions with Dr Jeffrey Burghardt (PNNL) were essential to the success of these experiments.

REFERENCES

Fleuchaus, P., et al. Worldwide application of aquifer thermal energy storage – A review. Renewable and Sustainable Energy Reviews, 2018.

Larson, S.A. Hydraulic fracturing in the Bohus Granite, SW Sweden: Tests for heat storage and heat extraction. GRC Annual Meeting, 1984.

Hellström, G. & Larson, S. Seasonal thermal energy storage – The HYDROCK concept. 2001.

Ramstad, R.K., et al. Ground source energy in crystalline bedrock – increased energy extraction using hydraulic fracturing in boreholes. 2007.

Janiszewski, M., Shen, B.T., & Rinne, M. Hydraulically fractured hard rock aquifer for seasonal storage of solar thermal energy. EUROCK, 2018.

Bloemendal, M., Olsthoorn, T., & Boons, F. How to achieve optimal and sustainable use of the subsurface for Aquifer Thermal Energy Storage. Energy Policy, 2014.

Hibbard, L., Burghardt, J.A., Sirota, D., Zhang, Y., Lecampion, B.T. and Linneman, D., 2024, December. Design and Operation of a Meso-Scale Fracture Thermal Energy Storage Test. In AGU Fall Meeting Abstracts (Vol. 2024, No. 1075, pp. H23G-1075).

Liu, D. and Lecampion, B. Laboratory investigation of hydraulic fracture growth in Zimbabwe gabbro. Journal of Geophysical Research: Solid Earth, 2022, 127(11), e2022JB025678.